Ultrasonic goniometric immersion tests for the characterization of fatigue post-LVI damage induced anisotropy superimposed to the constitutive anisotropy of polymer composites

Accepted Manuscript

Ultrasonic goniometric immersion tests for the characterization of fatigue post-LVI damage induced anisotropy superimposed to the constitutive anisotropy of polymer composites

Anna Castellano, Aguinaldo Fraddosio, Mario Daniele Piccioni

PII: S1359-8368(17)30330-X

DOI: 10.1016/j.compositesb.2017.02.025

Reference: JCOMB 4908

To appear in: *Composites Part B*

Received Date: 27 January 2017

Revised Date: 11 February 2017

Accepted Date: 14 February 2017

Please cite this article as: Castellano A, Fraddosio A, Piccioni MD, Ultrasonic goniometric immersion tests for the characterization of fatigue post-LVI damage induced anisotropy superimposed to the constitutive anisotropy of polymer composites, *Composites Part B* (2017), doi: 10.1016/j.compositesb.2017.02.025.

Ultrasonic goniometric immersion tests for the characterization of fatigue post-LVI damage induced anisotropy superimposed to the constitutive anisotropy of polymer composites

Anna Castellano[a,*], Aguinaldo Fraddosio[b], Mario Daniele Piccioni[b]

[a]*Dipartimento di Meccanica, Matematica e Management, Politecnico di Bari, Viale Japigia 182, 70126, Bari, Italy*

[b]*Dipartimento di Scienze dell'Ingegneria Civile e dell'Architettura, Politecnico di Bari, Via Orabona 4, 70125 Bari, Italy*

E-mail address:

[a,*]*anna.castellano@poliba.it*, [b]*aguinaldo.fraddosio@poliba.it*, [c]*mariodaniele.piccioni@poliba.it*

Abstract

We study an ultrasonic experimental approach for the damage characterization of polymer composites. Our approach is based on the key concept that damage of polymer composites involves a damage induced anisotropy superimposed to the constitutive anisotropy of the material. Thus, we correlate the damage to the analysis of the change in the anisotropy of the acoustic response of the material, by using an innovative goniometric ultrasonic immersion device designed and built at our laboratory. The experiments are performed on a glass fiber–reinforced composite material (GFRP), damaged first by a low velocity impact (LVI), and then by fatigue load cycles.

We first identify possible changes in symmetry axes (acoustic axes) and/or in the symmetry class of the material due to the damage; to this aim, we compare the velocity curves and the slowness curves of the composite before and after the damage. Then, starting from the velocity measurements acquired in goniometric ultrasonic immersion tests performed before and after the damage, we determine the variations of the elastic constants due to the damage. For a quantitative characterization of the damage, a suitable anisotropic damage model developed in the framework of the Continuum Damage Mechanics theory is employed. In this model, the damage is related to the relative variation of the elastic constants of the material.

For the validation of the procedure, ultrasonic results are also compared with experimental data obtained by conventional mechanical tests. The obtained results show the effectiveness of the proposed approach for the damage characterization of polymer composites.

Keywords:

A. Ultrasonic goniometric immersion test;

B. Damage induced anisotropy;

C. Polymer composites;

D. Slowness Surfaces;

E. Low Velocity Impact test.

1. Introduction

Today, non-destructive testing techniques play a crucial role for ensuring the integrity, and therefore the structural safety, of composite components in aerospatial, aeronautical, mechanical and civil constructions, during both the manufacturing and the service life. In particular, structural components made of polymer composites usually undergo cyclic different static and dynamic loads (compression, traction, shear, torsion, etc.), and sometimes also to the sudden action of impact loads. These loads may involve damage of the composite, which corresponds to a change of the mechanical behavior of the material. A typical damage process correspond to the development of microcracks; their nature and evolution depend on the loading type and on the mechanical properties of the composite [1]. For cyclic loads, generally microcracks are distributed rather uniformly; thus we have a diffuse damage. Conversely, for impact loads the damage is localized in limited area, and consist in concentrated microcracks, in intralaminar o interlaminar delaminations, fiber fractures, interface failures (fiber-matrix debonding), buckling of fibers, etc.. Whereas a broad literature on concentrated damage of composites exists, diffuse damage has received less attention by the researchers [2]. The propagation and the evolution of damage in composite components could lead to the failure, compromising the safety of the whole structure: this justify the relevance of the study of increasingly effective and capable experimental methods for the diagnosis and the monitoring of damage in composites [3-6].

Notice that the substantial progress recently made on theoretical and computational modeling of composite structures [7-11] have lead to the design of increasingly lighter and more efficient structures, for which of course the need of experimental methods for the monitoring of possible damages assumes an even more essential role.

In this context, ultrasonics represents a fast and effective non-destructive experimental technique for detecting defects and damage in composites structures (identification of cracks, microcracks, interlaminar voids, delamination, fracture matrix, etc.). For example, ultrasonic C-Scan tests are broadly employed for qualitative analyses of damage in composites. In these tests, suitable devices scan the surface of the component, and defects or damaged zones are associated to variations of the amplitude of ultrasonic waves travelling into the composite [12].

Thanks to new experimental approaches recently developed, and to the progress made in the theoretical modeling of the phenomena involved in ultrasonic experiments, ultrasonic tests allow for not only a merely "qualitative analysis", but also for a "quantitative analysis" of the damage [13,14]. In this vein, a key concept is that in anisotropic materials like composites defects like microcracks are characterized by their orientation with respect to the load direction and to material symmetry axes [15,16]. Thus, the damage induce an additional anisotropy superimposed on constitutive anisotropy of the composite [17,18]. Hence, the damage may be related to the damage induced anisotropy, and consequently the damage may be quantitatively evaluated by determining the variation of the symmetry axes (acoustic axes), and the variation of the degree of anisotropy of the composite [19,20].

Since ultrasonic tests are a very effective experimental tool for the characterization of the mechanical response of anisotropic materials [21], in principle those tests may also efficiently used for the quantitative evaluation of the damage in composites through the characterization of the damage induced anisotropy superimposed to the constitutive anisotropy. Anyway, this is a very complicated and ambitious research goal, because the identification of the anisotropic features of the damage requires the determination of all the elastic constants of the composite; moreover, it is necessary to distinguish the anisotropy due to the damage from the constitutive anisotropy. For overcoming these problems, the choice of suitable experimental procedures and of suitable theoretical models for the interpretation of experimental data it is needed. In particular, from an experimental point of view the use of contactless techniques like ultrasonic immersion techniques and ultrasonic laser techniques [21,22] allows for generating ultrasonic waves propagating along any direction into the composite, and then for probing the elastic response in any direction. Moreover, suitable anisotropic damage models, together with the reconstruction of the slowness surfaces and the velocity surfaces, may allow for quantitatively characterizing the damage. This also in the case, rather less tractable, of diffuse damage.

In this vein, here we propose a theoretical and experimental approach for the ultrasonic characterization of the damage induced anisotropy in fiber reinforced polymer composites. The experimental procedure is based on the use of an ultrasonic immersion goniometric device designed

and built by our laboratory (Laboratorio “M. Salvati”). By rotating a composite sample immersed into a water tank also housing the ultrasonic probes, it is possible to continuously vary the propagation direction of ultrasonic waves. Moreover, as predicted by the Snell law, by varying the angle of incidence between the ultrasonic beam and the sample surface it is possible to propagate any kind of polarized ultrasonic waves into the sample, both “pure” waves (longitudinal and shear waves) and “not pure” waves (quasi-longitudinal and quasi-shear waves). The latter are typical of acoustic behavior of anisotropic material. Thus, this goniometric device allows for experimentally facing two fundamental problems in the study of the mechanical response of materials: “the classification problem”, that is the characterization of the anisotropy class of a given material, and the “representation problem”, that is the determination of the independent elastic constants of a material once known its symmetry class.

Since the close correlation between the theoretical framework and the proposed experimental approach, in Section 2 we present a comprehensive enough outlook of the theoretical fundamentals; in particular, the characteristic acoustic surfaces are introduced, and the main aspects of the special case of wave propagation in transversely isotropic elastic materials are summarized.

Section 3 is devoted to the experimental tests on the glass fiber reinforced polymer composite under investigation. We first determine the anisotropy class of the material, and evaluate all the elastic constants needed for the description of its mechanical response. Then, we cause the damage of the composite by a low velocity impact followed by a tensile fatigue test. After the damage, we again perform ultrasonic immersion tests for evaluating the degree of anisotropy of the damaged composite, for determining the variation of the symmetry axes (acoustic axes), and for measuring the variation of the elastic constants due to the damage.

In Section 4 we employ the experimental data for the quantitative evaluation of the damage by adopting an anisotropic damage model proposed by Baste and Audoin [15,16] and developed in framework of the Continuum Damage Mechanics theory. Moreover, the damage is also studied by the comparison between the slowness curves and the velocity curves of the undamaged and of the damaged polymer composite.

The proposed approach proves to be very effective for the characterization of the damage in the examined GFRP composite; moreover, the comparison with the measurements obtained by conventional mechanical tests confirms the accuracy of the ultrasonic measurements.

2. Wave propagation in anisotropic elastic materials

2.1 Some fundamental concepts of the linear elastodynamic theory

From a theoretical point of view, wave propagation modeling in anisotropic elastic materials is a very well developed research subject [21,22] [24-26]. Since ultrasonic waves are viewed as small perturbations of the reference state (eventually prestressed), for the description of wave phenomena involved in the ultrasonic tests the linearized elastodynamic theory is usually employed. In other words, it is assumed that the material behave linearly elastically for these small perturbations. If the reference state is stress-free, the simpler linear elastodynamic theory may be applied.

Here we adopt the latter hypothesis, and we search for solutions of the equations of motion in the form of progressive plane waves. A plane wave is characterized by a displacement field of the form:

$$\mathbf{u}(\mathbf{x},t) = \mathbf{a}\,\varphi(\mathbf{x}\cdot\mathbf{n} - v\,t), \tag{1}$$

where: the vectors **a** and **n** represent the direction of motion and the direction of propagation, respectively; the scalar v represents the propagation velocity; φ is a real valued smooth function.

A plane wave is said to be a progressive elastic wave if it satisfies the fundamental equation of elastodynamic; that is, in absence of body forces, the following equation of motion:

$$\mathrm{Div}(\mathbb{C}[\nabla\mathbf{u}]) = \rho\ddot{\mathbf{u}} \tag{2}$$

where $\rho=\rho(\mathbf{x})$ is the mass density and $\mathbb{C}=\mathbb{C}(\mathbf{x})$ is the elasticity tensor (a fourth order tensor endowed by the first and second minor symmetry [24]). The Fresnel-Hadamard propagation condition [24] states that necessary and sufficient condition for the propagation of plane progressive elastic waves with propagation direction **n** and direction of motion **a** is that:

$$\left[\boldsymbol{\Gamma}(\mathbf{n}) - \rho v^2\mathbf{I}\right]\mathbf{a} = \mathbf{o} \tag{3}$$

where the second order tensor $\boldsymbol{\Gamma}(\mathbf{n})$ is called the Kelvin-Christoffel propagation tensor for the direction **n**, and is defined as

$$\boldsymbol{\Gamma}(\mathbf{n}) = \mathbb{C}^{t}[\mathbf{n}\otimes\mathbf{n}] \tag{4}$$

(the superscript "t" denotes the minor transposition operation for a fourth order tensor). By (4), the Christoffel tensor $\boldsymbol{\Gamma}(\mathbf{n})$ is related to the elastic properties of the material through the elasticity tensor $\mathbb{C}$, and to the direction of propagation **n**. From (3) it is clear that if an elastic wave propagates in a given direction **n**, then the square of the propagation velocity v is an eigenvalue of the Christoffel tensor (for the propagation direction **n**), while the direction of motion **a** is the associated eigenvector.

If the elastic tensor $\mathbb{C}$ is symmetric (that is, if $\mathbb{C} = \mathbb{C}^{T}$), then the Christoffel tensor $\boldsymbol{\Gamma}(\mathbf{n})$ is symmetric and admits for each direction of propagation **n** at least three real eigenvectors $\mathbf{a}_1, \mathbf{a}_2, \mathbf{a}_3$, with related eigenvalues v_1^2, v_2^2, v_3^2. Moreover, if the elastic tensor $\mathbb{C}$ is strongly elliptic (that is, if $(\mathbf{a}\otimes\mathbf{b})\cdot\mathbb{C}(\mathbf{a}\otimes\mathbf{b}) > 0, \forall\, \mathbf{a}\otimes\mathbf{b} \in \mathrm{Dya} - \{\mathbf{O}\}$, where Dya is the set of all the vectors dyads), then the Christoffel tensor is positive definite; consequently, the square roots of the eigenvalues are real, and therefore can be properly considered as wave propagation velocities. In the following, as usual in the linear elasticity theory, we admit that $\mathbb{C}$ is symmetric and positive definite, which imply that $\mathbb{C}$ is also strongly elliptic.

By (4), the features of the elasticity tensor $\mathbb{C}$ related to the symmetry properties of the elastic response of the material affect, through the Christoffel tensor $\boldsymbol{\Gamma}(\mathbf{n})$, the properties of progressive elastic waves propagating along a certain direction **n**. In particular, according to the polarization vector **a**, it is possible to have longitudinal waves, for which **a** and **n** are parallel, and transverse waves for which **a** and **n** are perpendicular. These kind of waves represent the so-called "pure" modes of wave propagation, which are the only kind of plane progressive waves supported by isotropic materials. Generally, also "not pure" modes of propagation are possible; in the latter case the polarization vector **a** is neither parallel nor perpendicular to the propagation direction **n**. In the literature "not pure" modes are often referred as quasi-longitudinal waves or quasi-shear waves, depending on the proximity of the direction of **a** to the direction of **n** or to a direction orthogonal to **n**. "Not pure" modes may propagate in materials that exhibit anisotropic mechanical behavior, due either to constitutive properties (so-called texture induced anisotropy) or to the damage (so-called damage induced anisotropy). More details on the polarization of elastic waves come from the Federov-Stippes theorem [24]: *if the elasticity tensor is symmetric and strongly elliptic, then at one point **x** there is at least an elastic longitudinal wave and two elastic transverse waves*. Furthermore, if the elasticity tensor $\mathbb{C}$ is symmetric and strongly elliptic, it is possible to show that if **e** is the unit

vector of an axis of material symmetry, then there exist an elastic longitudinal wave and two elastic shear waves whose direction of propagation is **e**.

2.2 The characteristic acoustic surfaces

In ultrasonic experiments on the mechanical characterization of anisotropic materials, the study of three families of characteristic acoustic surfaces: the "*velocity surfaces*" VS, the "*wavefront surfaces*" WS and the "*slowness surfaces*" SS, plays an important role. Each of these families of surfaces represents the variation with the propagation direction of the phase velocity, the energy velocity and the inverse of the phase velocity, respectively, of acoustic waves having each possible polarization. By restricting the study to the propagation in a certain plane, we get from the above surfaces three family of characteristic curves: "*velocity curves*" VC, the "*wavefront curves*" WC and the "*slowness curves*" SC, respectively.

Denoted with v the phase velocity[1], the "*velocity surface*" VS is the polar plot of the phase velocity vector $\mathbf{v}=v\mathbf{n}$ as a function of the direction of propagation **n** of a wave with a certain polarization. A family of three sheet of velocity surfaces can be defined: one for longitudinal waves and two for transversal waves. Notice that the longitudinal wave sheet contains both the transversal wave sheets because the phase velocity of longitudinal waves is always greater than the phase velocity of shear waves.

A "*slowness surface*" SS is the polar diagram of the inverse of the phase velocity as a function of the direction of propagation **n** of a wave with a certain polarization. By considering the three possible polarizations, a family of three sheet of slowness surfaces is obtained. A slowness surface is described by the *slowness vector* **s**, expressed as the ratio between the wave number vector **k** and the angular frequency ω:

$$\mathbf{s} = \frac{\mathbf{k}}{\omega} = \frac{\mathbf{n}}{v} \tag{5}$$

Since **s** and **v** are collinear and $s\,v=1$, where $s = |\mathbf{s}|$, the velocity surface and the slowness surface are related by an inversion through the origin. It is also possible to show that the energy velocity vector is normal to the slowness surface for each propagation direction.

A "*wavefront surface*" WS is the polar plot of the energy velocity vector $\mathbf{v}^e$ as a function of the direction of propagation **n** of a wave with a certain polarization. Since in Appendix A it is shown

[1] Some fundamentals about *phase velocity* v, *group velocity* $\mathbf{v}^g$ and *energy velocity* $\mathbf{v}^e$ are recalled in Appendix A.

that the group velocity $\mathbf{v}^g$ is equal to the energy velocity $\mathbf{v}^e$, a wavefront surface is also the polar plot with $\mathbf{n}$ of the group velocity vector $\mathbf{v}^g$. By considering the three possible polarizations, a family of three sheet of wavefront surfaces is defined. As it is shown in [26], the vector joining the origin to a point on the wavefront surface represents the distance travelled by the elastic energy in unit time. Moreover, the direction of propagation $\mathbf{n}$ of a plane wave having energy velocity $\mathbf{v}^e$ is normal to the wavefront surface. Finally, the direction of the energy velocity vector $\mathbf{v}^e$ (or, equivalently, of the group velocity vector $\mathbf{v}^g$) is skewed with respect to the wave number vector $\mathbf{k}$, which is always normal to the wavefront surface.

A slowness surface and the corresponding wavefront surface are related by:

$$\mathbf{v}^e \cdot \mathbf{s} = 1, \tag{6}$$

which links the energy velocity vector $\mathbf{v}^e$ to the slowness vector $\mathbf{s}$. Thus, a wavefront surface is the polar reciprocal to the corresponding slowness surface, that is, the direction of energy velocity vector $\mathbf{v}^e$ (or, equivalently, of the group velocity vector $\mathbf{v}^g$) indicates the normal direction to the slowness surface, and the direction of the phase velocity vector (i.e., the vector number $\mathbf{k}$) indicates the normal direction to the wavefront surface. In Fig. 1 we show a wavefront curve and the corresponding slowness curve; those curves are sections of the corresponding surfaces with a propagation plane.

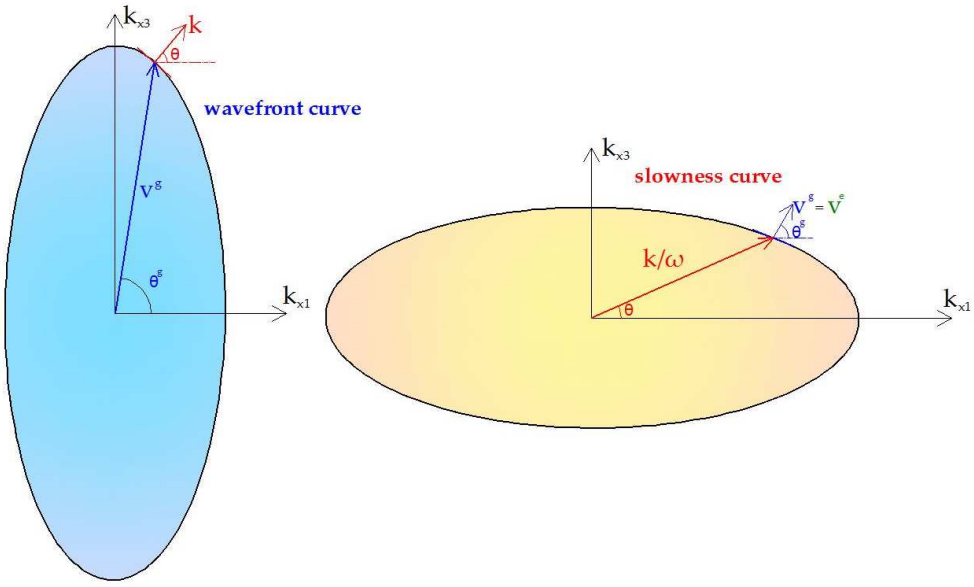

Fig. 1. Wavefront curve and slowness curve.

For isotropic materials, only pure waves propagate; then, we have three pure wave velocity surfaces. For anisotropic materials, instead, the three velocity surfaces refer generally to not pure waves (one quasi-longitudinal waves sheet and two quasi-transversal waves sheets), even though along certain directions (material symmetry axes) the propagating waves become pure. The same holds for the slowness surfaces and for the wavefront surfaces.

Moreover, since for isotropic materials the velocities of propagating waves do not depend on the directions of propagation **n**, each slowness surface consists in a sphere with radius equal to the inverse of the phase velocity. Since the normal to the surface of a sphere is collinear with its radius vector, phase and group velocity vectors are collinear. For anisotropic materials, instead, phase and group velocity vectors are no longer collinear and the shape of the slowness surfaces is no longer spherical, and may be very complex depending on the anisotropy features of the material. Each kind of material symmetry is related to a particular shape of the slowness surfaces [25]; thus, the slowness surfaces can be viewed as a "fingerprint" of the acoustic response of a material, and their experimental reconstruction allows for identifying the symmetry class of the examined material.

2.3 Wave propagation in transversely isotropic materials

For the purposes of the experimental analyses discussed in Section 3, we restrict our attention to the case of wave propagation in transversely isotropic linearly elastic materials. In particular, we consider a reference system such that the transverse isotropy axis coincide with the x_3-axis; thus, the elasticity tensor $\mathbb{C}$ have the following representation in Voigt notation

$$\mathbb{C} = \begin{bmatrix} C_{11} & C_{12} & C_{13} & 0 & 0 & 0 \\ C_{12} & C_{11} & C_{13} & 0 & 0 & 0 \\ C_{13} & C_{13} & C_{33} & 0 & 0 & 0 \\ 0 & 0 & 0 & C_{44} & 0 & 0 \\ 0 & 0 & 0 & 0 & C_{44} & 0 \\ 0 & 0 & 0 & 0 & 0 & C_{66} \end{bmatrix}, \tag{7}$$

with $C_{12} = C_{11} - 2C_{66}$.

In particular, for wave propagation in the x_1x_2 "isotropic" plane (π_{12} plane), orthogonal to the transverse isotropy x_3-axis, that is by assuming **n**=(cosφ, sinφ, 0), the Christoffel tensor (4) take the form:

$$\Gamma(\mathbf{n}) = \begin{bmatrix} C_{11}\cos\varphi^2 + C_{66}\sin\varphi^2 & (C_{11} - C_{66})\sin\varphi\cos\varphi & 0 \\ (C_{11} - C_{66})\sin\varphi\cos\varphi & C_{11}\sin\varphi^2 + C_{66}\cos\varphi^2 & 0 \\ 0 & 0 & C_{44} \end{bmatrix}, \tag{8}$$

and it is possible to show that only a pure longitudinal wave and two pure transversal waves may propagate (see [21]). Thus, the velocities of propagating ultrasonic waves do not depend on the direction of propagation **n**. If we consider instead the propagation of ultrasonic waves in the x_1x_3 plane (π_{13} plane), which contain the transverse isotropy x_3-axis, that is by assuming **n**=(cosφ, 0, sinφ), the Christoffel tensor (4) take the form:

$$\Gamma(\mathbf{n}) = \begin{bmatrix} C_{11}\cos\varphi^2 + C_{44}\sin\varphi^2 & 0 & (C_{13}+C_{44})\sin\varphi\cos\varphi \\ 0 & C_{44}\sin\varphi^2 + C_{66}\cos\varphi^2 & 0 \\ (C_{13} + C_{44})\sin\varphi\cos\varphi & 0 & C_{44} + (C_{33}-C_{44})\sin\varphi^2 \end{bmatrix}. \tag{9}$$

Now, wave velocity depends on the direction of propagation **n**. Indeed, by evaluating the eigenvalues and the eigenvectors of the Christoffel tensor (9), we see that for each direction of propagation **n** a quasi-longitudinal wave (QL), a pure transversal wave (T) and a quasi-transversal wave (QT) are possible, and that their slowness depend on **n** through the angle φ:

$$s_{QL} = \frac{1}{\sqrt{\frac{A+\sqrt{A^2 - 4B}}{2\rho}}}, \quad s_T = \frac{1}{\sqrt{\frac{C_{44}\sin^2\varphi + C_{66}\cos^2\varphi}{\rho}}}, \quad s_{QT} = \frac{1}{\sqrt{\frac{A - \sqrt{A^2 - 4B}}{2\rho}}}, \tag{10}$$

where

$$\begin{aligned} A &= C_{11}\cos^2\varphi + C_{33}\sin^2\varphi + C_{44} \\ B &= (C_{11}\cos^2\varphi + C_{44}\sin^2\varphi)(C_{44}\cos^2\varphi + C_{33}\sin^2\varphi) - (C_{13} + C_{44})^2\sin^2\varphi\cos^2\varphi. \end{aligned} \tag{11}$$

Fig. 2 shows the theoretical velocity surfaces VS and slowness surfaces SS, respectively, of a transversely isotropic material; those surfaces are obtained by plotting the slowness (10) as a function of the direction **n**. In Fig. 2, the depicted surfaces are sectioned by π_{13} plane; moreover, we denote with different colors the surfaces related to the differently polarized ultrasonic waves: blue for quasi-longitudinal waves; green for pure transversal waves; red for quasi-transversal waves.

Notice that the slowness surfaces for a transversely isotropic elastic material are rotationally symmetric about the x_3-axis (axis of transverse isotropy), and have reflection symmetry about the π_{12} plane [27].

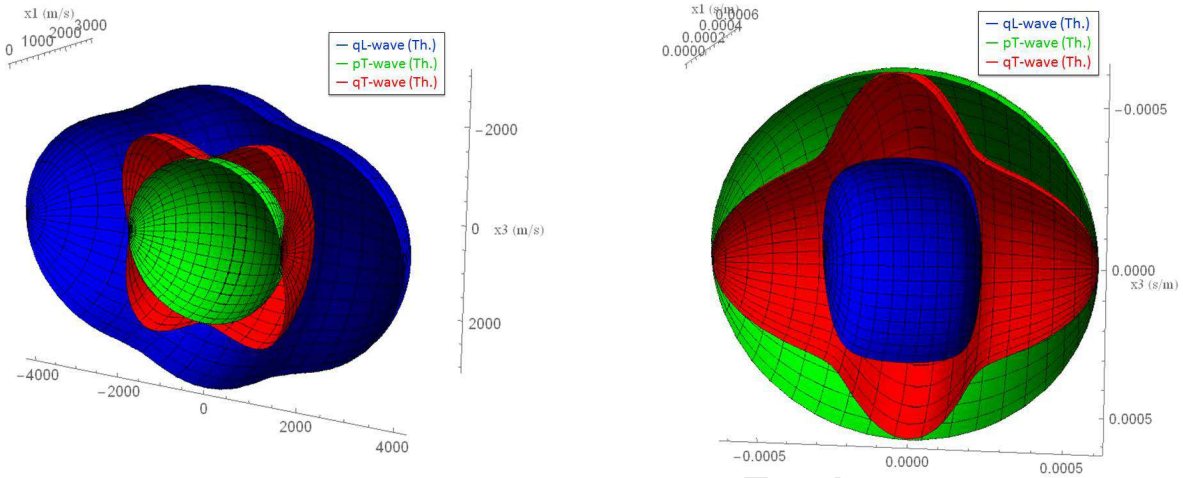

(a) (b)

Fig. 2. Transversely isotropic materials; transverse isotropy axis=x_3-axis. (a) velocity surfaces VS; (b) slowness surfaces SS.

2.4 Ultrasonic goniometric experimental procedures for the mechanical characterization of materials

The theoretical framework in Sect. 2.1-2.3 suggests an experimental counterpart in terms of ultrasonic non-destructive tests for the characterization of the mechanical response of materials. Indeed, the study of the Christoffel equation (3) allows for addressing two fundamental problems of the mechanics of elastic materials: the "*classification problem*", that is the determination of the degree of anisotropy of a given material (determination of the symmetry class and identification of the material symmetry axes), and the "*representation problem*", that is (once known the symmetry class) the determination of the elastic moduli needed for the description of the elastic response.

In particular, starting from experimental measures of the velocities of ultrasonic waves travelling in various directions in the material and having different polarizations, it is possible to experimentally reconstruct the slowness surfaces of a material: this allows for identifying the symmetry class of the material, and for determining the material symmetry axes. Notice that the material symmetry axes coincide with the acoustic axes; then, these axes are characterized by the following properties [25]: 1) for each propagation mode, the direction of phase velocity coincides with the direction of group velocity; 2) according to the theorem of Federov-Stippes, for some symmetry classes (for example, in the case of transverse isotropy) transverse waves propagating along a material symmetry axis have the same velocity.

Once known the symmetry class of a material, the inversion of the Christoffel equation (3) allows for determining all the independent components of the elastic tensor. To this aim, after having experimentally measured the velocity of an ultrasonic wave propagating in a certain direction and having a certain polarization, (3) gives a non-linear equation in the elastic constants [25]. Thus, starting from experimental measures of the velocities of ultrasonic waves propagating in suitable directions and having suitable polarizations, it is possible to get a set of non-linear equations in the unknown elastic constants. For the solution of those equations, two fundamental issues have to be addressed. First, the propagation directions to be considered in the experiments have to be suitably chosen in order to have access to all the elastic constants. For example, if we consider the case of transversely isotropic elastic materials, (8) shows that for waves propagating in the "isotropic plane" (the plane orthogonal to the transverse isotropy axis) the Christoffel tensor involves only three of the five independent elastic constants. Thus, in order to get equations also involving the other two elastic constants, different direction of propagation have to be examined; for example, (9) shows that directions lying in a plane containing the transverse isotropy axis could be considered. The second issue is typical of inverse methods for the identification of physical parameters based on experimental measurements: since uniqueness problems may arise, and in order to minimize the errors in the parameters identification due to experimental errors and data dispersion, it is usual to perform a number of measures significantly large with respect to the number of the parameters to be identified, and then to adopt numerical procedures aimed at recovering the parameters by minimizing the errors, like optimization methods [15] [27,28].

For the above discussion, in ultrasonic experiments for the mechanical characterization of anisotropic materials the need to examine propagation properties in different directions suggests the employ of goniometric ultrasonic techniques. The latter are based on suitable experimental devices aimed at rotate the ultrasonic probes and/or the specimen. Moreover, for experimental convenience goniometric ultrasonic tests are preferentially performed without a direct coupling between the ultrasonic probes and the specimen, that is by using experimental setups based on immersion techniques [21,22] [30] or other techniques like laser ultrasonic [23] or air-coupled ultrasonic [31].

Today, goniometric ultrasonic tests can be consider one of the most effective, versatile and reliable technique for the mechanical characterization of anisotropic materials [21,22] [30] [32]. We underline that this technique allows for the classification of the anisotropy class of the material in a non-destructive and relatively uncomplicated way, differently from other techniques like mechanical tests. Moreover, the latter require the use of a large number of specimens, and normally require a priori assumptions on the anisotropy class in order to design and perform the experiments.

Finally, since the characterization of the damage can be performed through the analysis of the anisotropic features of the changes of the mechanical response, goniometric ultrasonic tests are very effective also for the analysis of the damage of anisotropic material. To this aim, the damage induced anisotropy superimposed on the constitutive anisotropy of the material has to be experimentally studied [33-36]. In particular, it is possible to characterize the damage starting from the evaluation of the variation of the anisotropic features of the elastic response and from the variation of the anisotropic elastic constants. An useful tool for studying the variation of the anisotropy of the material are the slowness surfaces and the velocity surfaces, which allow for easily visualizing the changes due to the damage. For the sake of simplicity, frequently the slowness curves (or the velocity curves), which are sections of the slowness surfaces (or of the velocity surfaces) with a propagation plane, are examined.

3. An ultrasonic goniometric immersion procedure for the mechanical characterization of polymer composites

3.1 Experimental setup

The ultrasonic tests below described were carried out by using an innovative ultrasonic goniometric immersion device designed and built by Laboratory “M. Salvati” of Politecnico di Bari [21,22]. This ultrasonic device has been specifically designed for the mechanical characterization of anisotropic materials. Indeed, this goniometric device allows for analyzing the features of the propagation of ultrasonic waves in different directions. For the reasons explained in Sect. 2.4, it is then possible to determine the material symmetry axes (*classification problem*) and the components of the elastic tensor (*representation problem*). Moreover, the ultrasonic goniometric approach can be employed for evaluating the damage through the characterization of the damage induced anisotropy, that is, by analyzing the variation of the anisotropic features of wave propagation from the undamaged state to the damaged state.

The above mentioned ultrasonic goniometric immersion device (shown in Fig. 4) consists in: an immersion water tank; a frame housing ultrasonic immersion transducers and/or a reflective surface in Plexiglas; a rotating sample slot operated by a stepper motor. A reducer gearbox enables us to rotate the sample with very small angular steps (0.036°): according to the Snell’s law, this allows for accurately generating and analyzing any kind of polarized ultrasonic (“pure” and “not pure”) waves into the material for any direction of propagation, in a principal symmetry plane or in a

generic plane. Moreover, for enhancing the versatility of the experimental setup, the device can be used in two different configurations: through-transmission tests, with two opposite ultrasonic probes (transmitter and receiver), and back-reflection tests, with only one probe, acting at the same time as transmitter and receiver, opposite to a reflective surface.

In this paper, we report experimental results obtained in back-reflection tests configuration. In particular, ultrasonic waves are generated and received by an unfocused ultrasonic probe with a central frequency of 1 MHz. The ultrasonic signals are handled by an ultrasonic pulser/receiver Olympus 5072PR and an oscilloscope Agilent DSO6014A (100 MHz, 4 channels).

The ultrasonic experiment is fully controlled (from the management of the stepper motor up to the stage of the analysis and the processing of ultrasonic signals) by a LabVIEW software ad hoc designed [21,22]. Moreover, the LabVIEW software extracts the data on the wave velocities required for the mechanical characterization of the material. To this aim, for each rotation angle of the sample, the software measures the time of flight (TOF) Δt of ultrasonic waves by the cross-correlation between the auto-correlated reference signal (ultrasonic signals acquired in water without the sample) and the average of the normalized signals acquired (ultrasonic signals acquired with the sample placed in the slot). Then, for a given angle of incidence θ of the ultrasonic beam on the surface of the sample, the LabVIEW software evaluate the phase velocity v_p of ultrasonic waves propagating into the sample by the following expression, which is valid for the back- reflection technique [21-22] [32]:

$$v_p = \left[\left(\frac{\Delta t}{2d} \right)^2 - \frac{\Delta t / d}{v_w} \cos\theta + \left(\frac{1}{v_w} \right)^2 \right]^{-1/2} \tag{12}$$

where: d is the thickness of the sample; v_w is the ultrasonic velocity in water (about 1,473 m/s). At the end of each ultrasonic test, when the entire prearranged rotation angle of the sample has been completed, the LabVIEW software displays a graph showing the measured ultrasonic phase velocities v_p (m/s) versus the angle of incidence θ (deg) of the ultrasound beam on the surface of the sample.

3.2 The glass fiber-reinforced polymer sample details

We study the propagation of ultrasonic waves in a sample of a glass fiber–reinforced composite material (GFRP). In particular, the composite material is made of 4 unidirectional fiberglass reinforced layers of Orthophthalic Distitron I 100 SV1.5 Polyester matrix, with an overall thickness

of 3.8 mm. This GFRP composite is specifically designed for the construction of innovative wind turbine blades, developed within a research project on more efficient wind renewable energy production.

Unidirectional fiber–reinforced composites like those under investigations are usually modeled as transversely isotropic linearly elastic material, with the transverse isotropy axis coincident with the axis of the fibers. In the following, we assume a reference system with x_3-axis parallel to the axis of the fibers as depicted in Fig. 3; thus – after having experimentally confirmed that the material actually behave as transversely isotropic – we can refer to the theoretical framework developed in Sect. 2.3.

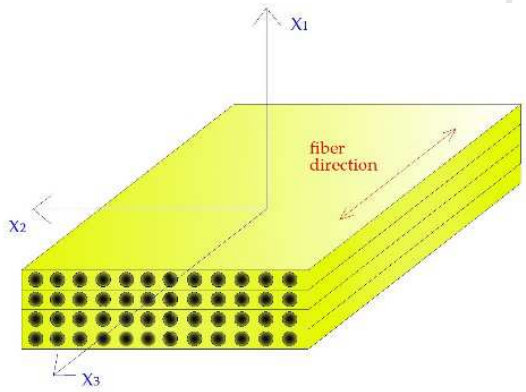

Fig. 3. Unidirectional glass-fiber reinforced composite (GFRP).

Once determined the mass density ρ of the GFRP composite, by the inversion of the Christoffel equation (3) the velocity data recorded in the ultrasonic goniometric tests allow us to determine the five elastic independent constants (C_{11}, C_{13}, C_{33}, C_{44} and C_{66}) needed for the description of the elastic behavior of the GFRP composite material.

In particular, since we have to characterize the mechanical response of a transversely isotropic material, we have to propagate ultrasonic waves in two different planes (see Sect. 2.3-2.4): one is the isotropic plane $\pi_{12,}$ which allows us to measure the elastic constants C_{11}, C_{44} and C_{66}; the other is the plane π_{13} (a plane containing the fibers), which allows us to measure also C_{33} and C_{13}. Thus, we performed the experimental analysis by arranging the GFRP sample in the slot of the goniometric device in two different configurations (Fig. 4): the first configuration is such that the rotation axis of the sample is parallel to x_3-axis (i.e., the fiber axis), so that ultrasonic waves propagated in the plane π_{12}. In the second configuration the sample was placed with the rotation axis orthogonal to the axis of the fibers, and coincident with the x_2-axis, so that the propagation of ultrasonic waves took place in the plane π_{13}.

Sufficiently large overall rotations of the GFRP sample (up to 25°) have been considered in order to obtain the mode conversions needed – according to the Snell's law – for generating each kind of ultrasonic polarized waves, whose velocities have to be measured.

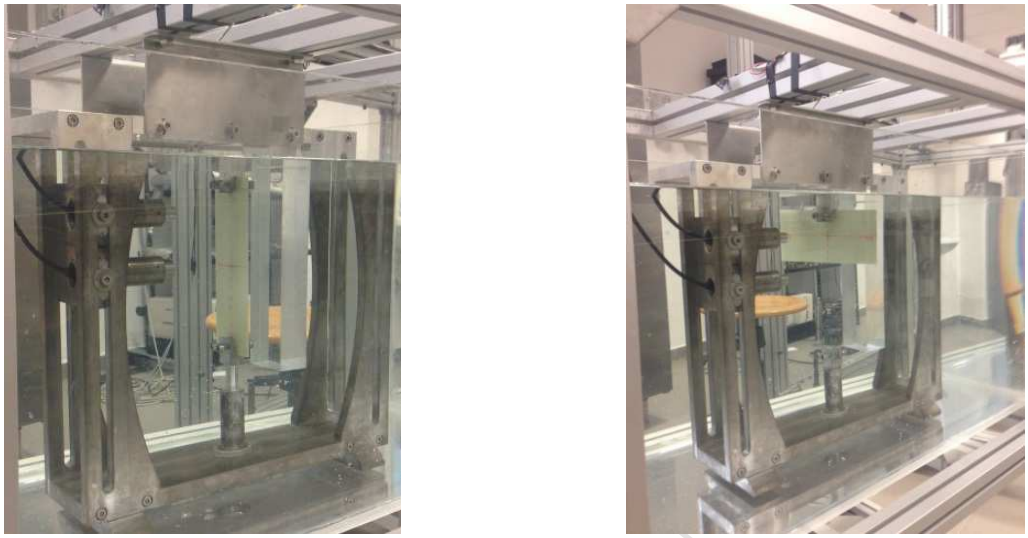

(a) (b)

Fig. 4. (a) first test configuration: propagation in plane π_{12} and sample rotation around x_3-axis; (b) second test configuration: propagation in plane π_{13} and sample rotation around x_2-axis.

3.3 Mechanical characterization of the undamaged glass fiber-reinforce polymer composite

First, we performed ultrasonic goniometric immersion tests on the undamaged GFRP sample. Fig. 5 shows the graph phase velocity-incident angle obtained as the result of the analysis performed in the propagation in the isotropic plane π_{12}, orthogonal to the fibers (first test configuration). We observe that, according to the Snell's law, ultrasonic longitudinal waves propagate in the sample until the first critical angle (approximately 12.5°) is reached. In the plane π_{12} the velocity of longitudinal waves do not depend on the angle of incidence θ; thus we have pure longitudinal waves as it normally occurs in isotropic materials. After the first critical angle, we notice some spurious echoes, not representative of the actual mechanical behavior. After these spurious echoes, the acquired signals correspond to the propagation of shear waves into the sample; in particular, we have pure shear waves, since their velocity is almost constant as θ varies.

Fig. 6 shows the graph phase velocity-incident angle obtained as the result of the analysis performed in the propagation plane π_{13}, parallel to the fibers (second test configuration). For small incident angles, we expect the propagation of quasi-longitudinal ultrasonic waves into the sample until the first critical angle (approximately 15.4°) is reached. In the plane π_{13} we notice that the velocity of longitudinal waves slightly depends on the angle of incidence θ (this is typical of quasi-

longitudinal waves). After the first critical angle, we observe two different kind of shear waves: first, we observe quasi-shear waves, since the velocity varies with the angle of incidence θ. After a second critical angle (approximately 21.2°), pure shear waves, whose velocity is almost constant as θ varies, propagate.

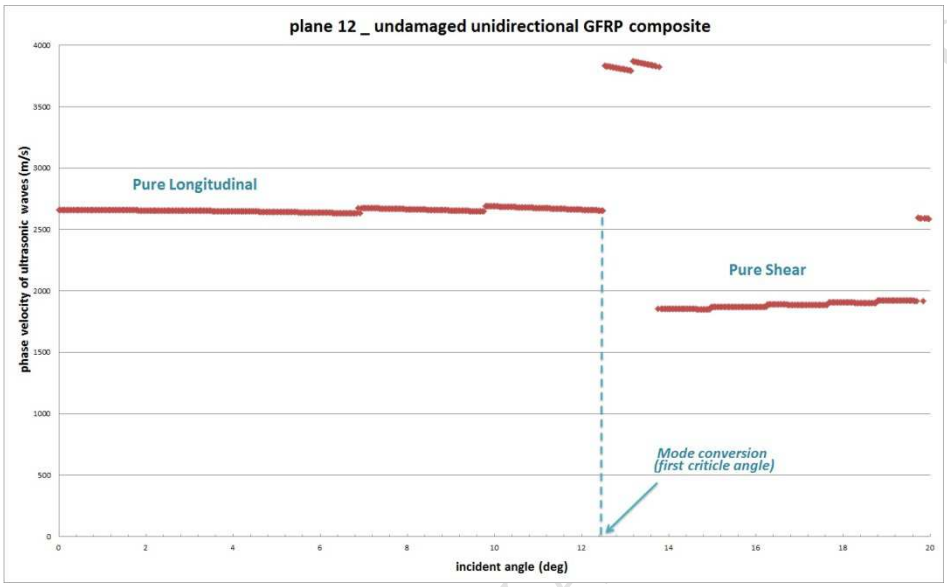

Fig. 5. Ultrasonic phase velocity-incident angle (plane π_{12}, undamaged composite).

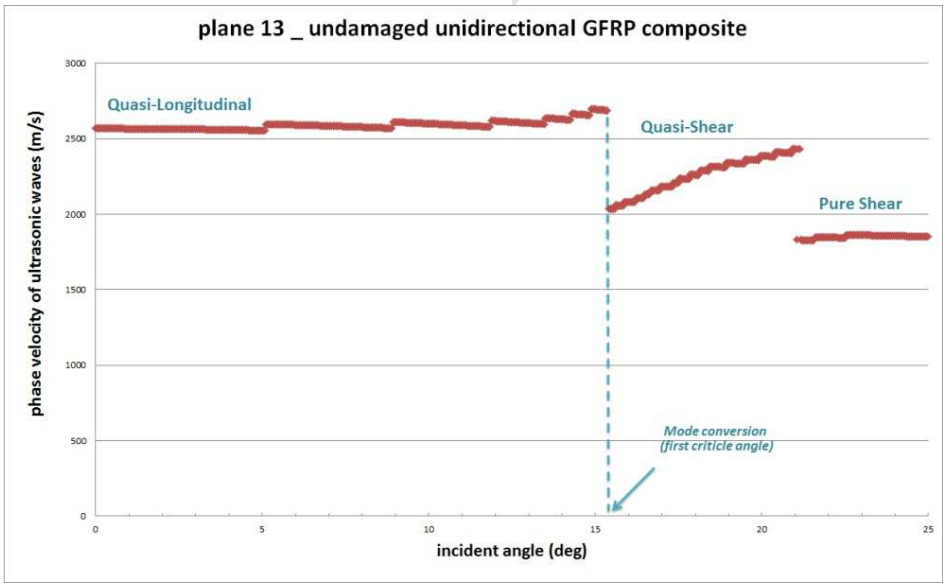

Fig. 6. Ultrasonic phase velocity-incident angle (plane π_{13}, undamaged composite).

The acquired ultrasonic velocity data allow us for verifying if the assumed hypothesis of transversely isotropic elastic behaviour actually corresponds to the observed acoustic response of the sample. To this aim, we determine the theoretical slowness curves in the hypothesis of

transverse isotropy, and we see that the experimentally reconstructed portions of the slowness curves fit sufficiently well the theoretical previsions. Fig. 7 reports the comparison between the experimental and the theoretical slowness curves for propagation in the plane π_{13}. Once figured out the classification problem on the base of the experimental data, we can refer to the model of transversely isotropic elastic material for the purposes of subsequent analyses.

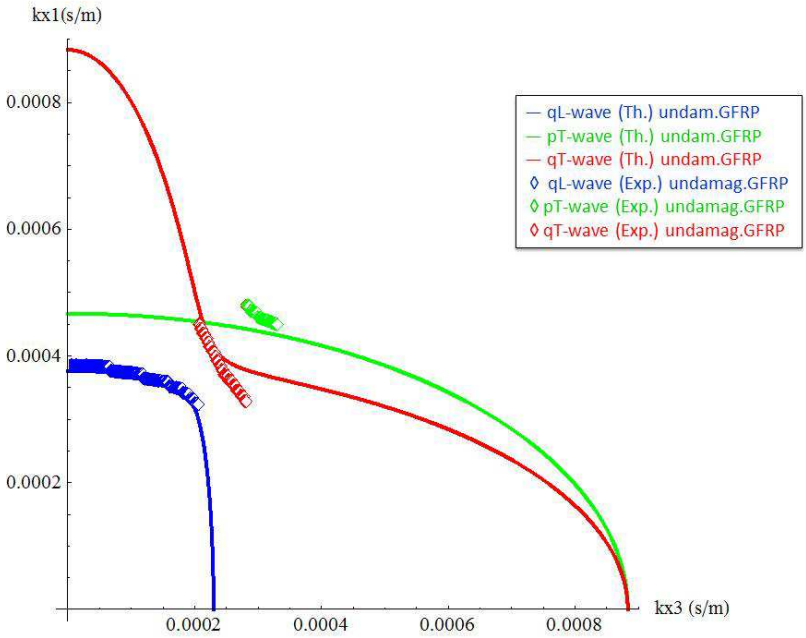

Fig. 7. Comparison between experimental and theoretical slowness curves (plane π_{13}, undamaged composite).

In particular, once measured the mass density of the GFRP composite (ρ=1,740 kg/m^3), we can determine by the inversion of the Christoffel equation (3), written for the case of transversely isotropic elastic materials, the 5 elastic constants of the undamaged composite material (representation problem).

Since we have a redundant set of experimental data, for enhancing the precision of the determination of the elastic constants we performed a last square regression analysis, minimizing the errors between experimental and theoretical values. The obtained values of the elastic constants are collected in Table 1.

Table 1

Elastic constants of the undamaged GFRP composite (GPa).

C_{11} (GPa)	C_{33} (GPa)	C_{44} (GPa)	C_{66} (GPa)	C_{13} (GPa)
12.29	32.96	2.23	7.98	2.26

Moreover, we determine starting from the ultrasonic measurements the Young modulus in the direction of the fibers (x_3-axis): E_3=31,367 MPa. The latter is in a very good agreement with the value of E_3 obtained by a conventional mechanical tensile test: E_3=31,20 MPa.

3.4 Low velocity impact (LVI) and fatigue post-LVI damage of the sample

The GFRP sample was damaged by two artificial damage tests aimed at reproducing possible damages of the GFRP composite during the service life of structural components. In particular, the artificial damage is aimed at reproducing a low velocity impact (LVI) on a GFRP composite structural component (for example, in the case of wind turbine blades, the impact of a hailstone), after which the component remain in service before the inspection and the maintenance. Is then important to analyze, subsequently to the LVI induced damage, the evolution of the damage induced by fatigue loads.

The low velocity impact (LVI) test has been performed by a custom-made facility with a hemispherical impactor with diameter 10 mm, impacting the surface of the sample in the direction named x_1 (see Fig. 3). We measured an impact energy level of 7 J. The use of a low value of the impact energy is justified, among other things, because we do not want to break the specimen.

After the LVI test, we performed a fatigue tensile test in order to induce in the sample a post-LVI fatigue damage. In the fatigue test, the specimen was subjected to different and increasing fatigue load levels by a MTS uniaxial fatigue testing machine; the fatigue loads have been applied in the direction of the axis of the fibers (x_3 direction). In particular, we fixed the ratio between the maximum and the minimum stress $R=\sigma_{max}/\sigma_{min}=0.1$, and we performed 10^4 load cycles with σ_{max}=67 MPa followed by 10^4 load cycles with σ_{max}=78 MPa, by 10^4 load cycles with σ_{max}=100 MPa, and by 10^4 load cycles with σ_{max}=122 MPa.

Fig. 8 show both the undamaged GFRP sample and the damaged GFRP sample as it appears at the end of the fatigue post-LVI damage test. For the damaged sample, we have highlighted in red the very visible impact area and a fracture occurred near the gripping area.

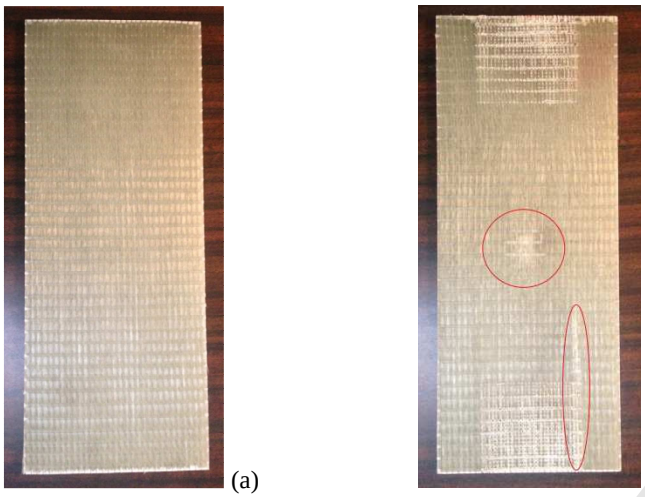

(a) (b)

Fig. 8. Undamaged (a) and fatigue post-LVI damaged GFRP sample (b).

3.5 Mechanical characterization of the damaged glass-fiber reinforced polymer composite

After the two damage tests, we have again analyzed the acoustic response of the sample by means of ultrasonic goniometric immersion tests; Fig. 9 and Fig. 10 show the acoustic behavior of the GFRP sample after the damage. In particular, Fig. 9 shows the graph phase velocity-incident angle obtained for ultrasonic wave propagation in the plane π_{12}, orthogonal to the fibers (first test configuration). Pure longitudinal waves, having almost constant velocity as θ varies, propagate into the sample until the first critical angle is reached (approximately 9.3°). The latter is different from the first critical angle measured for the undamaged sample (see Fig. 5). After the first critical angle, we observe (approximately up to θ=15.9°) the presence of some velocity measurements which cannot be considered "spurious echoes", as in the case of the undamaged composite (see Sect. 3.3). Instead, we assume that the damage suffered by the sample has compromised the integrity of the Polyester matrix. Thus, we ascribe these spurious velocity measurements to the presence of discontinuities in the matrix; this hypothesis should be confirmed by suitable micromechanical investigations. After θ=15.9° quasi-shear waves, whose velocity depend on the angle θ, propagate into the sample.

Fig. 10 shows the graph phase velocity-incident angle obtained in the second test configuration (propagation in the plane π_{13}). Ultrasonic quasi-longitudinal waves, with the velocity dependent on the incident angle θ, propagate into the sample until the first critical angle is reached (approximately 16.6°). Again, the value of the first critical angle is different from that observed for the undamaged sample (see Fig. 6). Then, we have quasi-shear waves, whose velocity depend on the angle θ. Finally, after a second critical angle (approximately 23.1°), pure shear waves, whose velocity is

almost constant as θ varies, propagate. We notice that also the second critical angle differs from that observed for the undamaged sample (see Fig. 6).

Now, since the damage involves a damage induced anisotropy superimposed on the initial transverse isotropy of the composite, we need to verify if the impact load and the subsequent fatigue cycles have changed the symmetry class of the material. We recall that the impact load has acted along a direction (x_1 direction) orthogonal to the principal axis of transverse isotropy (x_3 direction); anyway, the energy of the impact has been very low. Then, fatigue loads have been applied in the direction of the axis of the fibers (x_3 direction). Given the above, we expect that the damage induced anisotropy results in a change of the degree of anisotropy of the material, but not in a change of its symmetry class. In other word, compared to the undamaged material we expect that after the damage the material continues to behave as transversely isotropic, but the anisotropic behavior become more pronounced, especially in x_1 direction. Also, we expect a change in the values of the elastic constants.

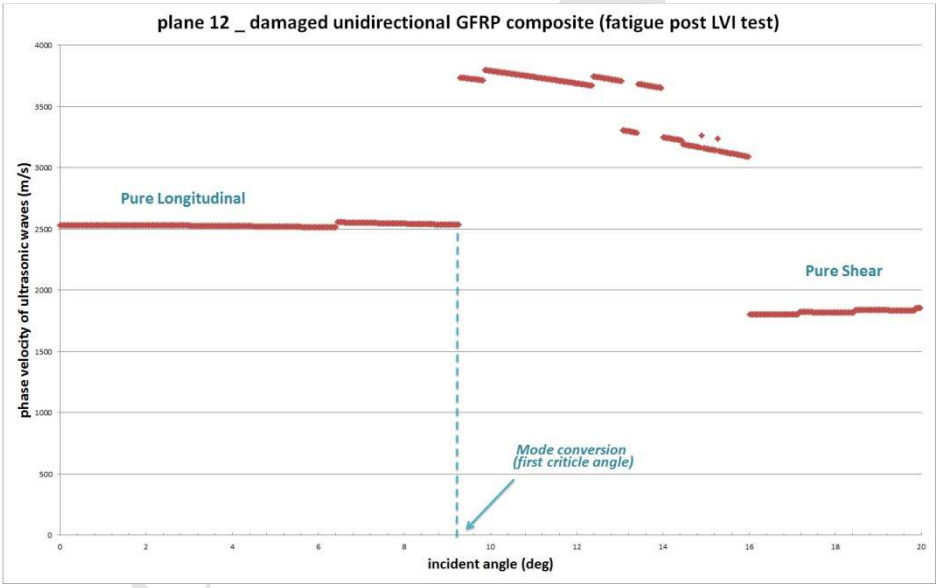

Fig. 9. Ultrasonic phase velocity-incident angle (plane π_{12}, damaged composite).

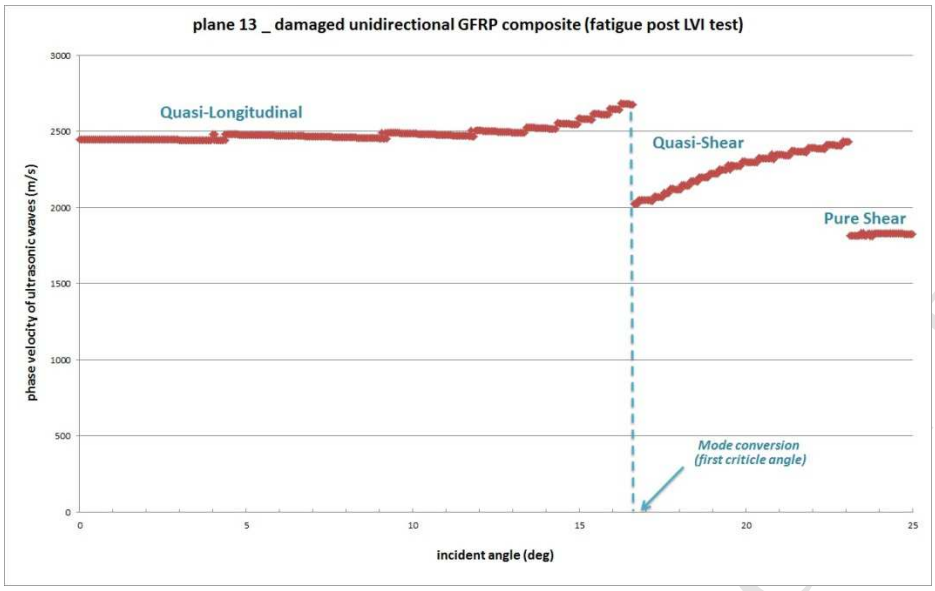

Fig. 10. Ultrasonic phase velocity-incident angle (plane π_{13}, damaged composite).

In order to verify the above assumptions, we again classify the symmetry properties of the elastic response by comparing the theoretical slowness curves, determined in the hypothesis of transverse isotropy, with the obtained experimental data. As Fig. 11 (which refers to propagation in the plane π_{13}) shows, the agreement between theoretical previsions and experimental data is quite good; thus, we can still refer to the model of transversely isotropic elastic material for the purposes of subsequent analyses.

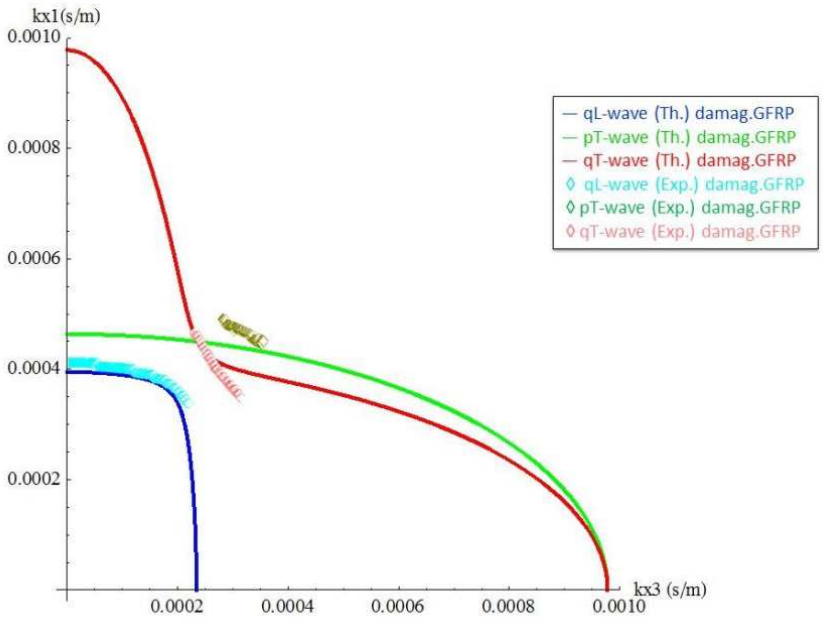

Fig. 11. Comparison between experimental and theoretical slowness curves (plane π_{13}, damaged composite).

Finally, starting from the velocity measurements and from the measured density of the material (ρ=1,740 kg/m^3), we determine by the inversion of the Christoffel equation (3), again written for transversely isotropic elastic materials, and by a last square regression analysis (see Sect. 3.3), the 5 elastic constants of the damaged composite material. Those constants are collected in Table 2.

Table 2

Elastic constants of the fatigue post-low velocity impact test damaged composite (GPa).

C_{11} (GPa)	C_{33} (GPa)	C_{44} (GPa)	C_{66} (GPa)	C_{13} (GPa)
11.16	31.77	1.82	8.10	2.85

Also for the damaged composite, in order to verify the accuracy of the ultrasonically determined elastic moduli, we calculate from the above data the Young modulus E_3 in the direction of the fibers (x_3-axis): E_3=29,120 MPa. Then, we determine the same elastic modulus by a conventional mechanical tensile test; the obtained value, E_3=28,970 MPa, is nearly coincident with the ultrasonically determined one.

4. Ultrasonic characterization of the damage for the GFRP composite

4.1 Quantitative analysis of the damage for anisotropic composites

In the classical Continuum Damage Mechanics (CDM) theory [37-39], the damage is quantitatively evaluated on a macroscopic scale by measuring the specific change of the elastic constants. For example, for isotropic materials a scalar damage variable related to the relative change of the Young modulus is employed. Here, due to the constitutive anisotropy of composite materials, for a quantitative evaluation of the damage mechanical models based on tensorial damage measures have to be used. These models allow for estimating the damage induced anisotropy superimposed to the constitutive anisotropy of the composite. In particular, we adopt a damage model proposed by Baste and Audoin in [10], developed in the framework of the CDM theory, and based on a tensorial damage measure **D** whose components are related to the specific stiffness constants variation. This model is general since it is applicable independently of the fibers reinforcement nature, of the geometry and types of microcracks, interlaminar voids and delaminations, and of failure mechanisms of the composite. Moreover, this model have a phenomenological character since the determination of the damage is directly related to some measured quantities in ultrasonic

goniometric immersion tests (i.e., to the phase velocities of ultrasonic waves) through the anisotropic tensorial damage measure [17-20]. In particular, we have

$$D_{ii} = 1 - \frac{\tilde{C}_{ii}}{C_{ii}}, \quad i=1,2,...,6 \qquad \text{(diagonal terms)} \tag{13}$$

$$D_{ij} = \frac{C_{ij} - \tilde{C}_{ij}}{C_{ij} + \text{sign}\left(C_{ij} - \tilde{C}_{ij}\right)\sqrt{C_{ii}\left(1-D_{ii}\right)C_{jj}\left(1-D_{jj}\right)}}, \quad i, j=1,2,...,6, \quad i \neq j, \quad \text{(off-diagonal terms)} \tag{14}$$

The wavy stiffness constants refer to the damaged material, while the unmarked stiffness constants refer to the undamaged material. Theoretically, if the norm $|\mathbf{D}|$ of the damage tensor $\mathbf{D}$ is equal to 0, the material is not damaged; if $0<|\mathbf{D}|<1$, some damage happens; if $|\mathbf{D}|=1$, the material is totally damaged.

The comparison between the graphs phase velocity-incident angle obtained by goniometric immersion ultrasonic tests for the GFRP composite before and after the fatigue post-LVI impact damage shows significant variations in the acoustic response due to the damage. This comparison already allows us to perform a qualitative assessment of the occurred damage.

Here, by employing the damage model above summarized, we carry out a quantitative analysis of the damage. In particular, starting from the values of the elastic constants collected in Table 1 (undamaged material) and in Table 2 (damaged material), we determine by (13)-(14) the components of the tensorial damage measure $\mathbf{D}$. The latter are collected in Table 3.

Table 3

Components of the damage tensor $\mathbf{D}$.

$\mathbf{D_{11}}$	$\mathbf{D_{33}}$	$\mathbf{D_{44}}$	$\mathbf{D_{66}}$	$\mathbf{D_{12}}$	$\mathbf{D_{13}}$
0.092	0.036	0.184	-0.015	0.014	0.181

We get that the norm of the tensorial damage measure is $|\mathbf{D}|=0.153$. The comparison between the values of the elastic constant in Tables 1-2, as well as the examination of the values of the components of $\mathbf{D}$, shows that the effects of the fatigue post-LVI damage entail essentially the following aspects. First, we observe the reduction of the elastic constant C_{11} related to the extensional behavior in the direction x_1 (direction of the impact); according, we have $D_{11}=0.092$. Moreover, we have a relatively larger reduction of the elastic constants C_{44} related to the shear behavior in the planes π_{12} and π_{23} (the latter is orthogonal to the direction of the impact); according, we have $D_{44}=0.184$. Finally, an increase of the elastic constant C_{13} expressing the coupling between

extensional deformations in the directions orthogonal to the fibers (x_1 and x_2 directions) and the normal stress in the direction of the fibers (x_3 direction); correspondingly, we have D_{13}=0.181. The variation of the elastic constant C_{33}, related to the extensional behavior in the direction x_3 (direction of the fatigue loads), is relatively small since D_{33}=0.036.

Finally, we observe that D_{66} come back to be negative (D_{66}=-0.015): this does not violate any theoretical assumption or requirement on the tensorial damage measure **D** (see, also [33,34] [36]).

4.2. Damage induced anisotropy: analysis of the characteristic acoustic curves

The analysis of the change in the anisotropy of the GFRP sample due the fatigue post-LVI damage is also performed by the comparison between the characteristic acoustic curves of the undamaged and the damaged composite.

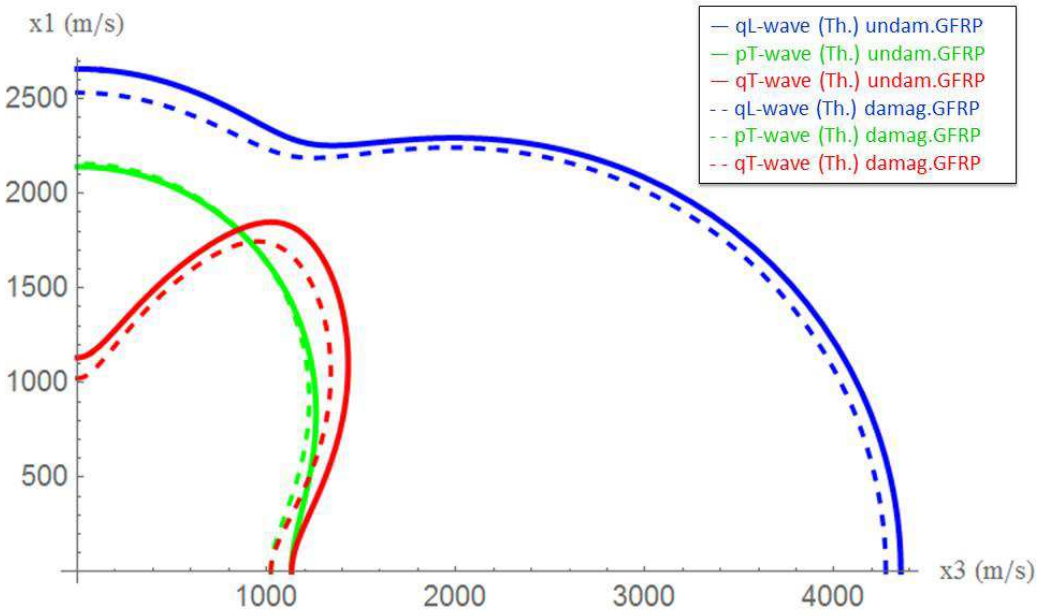

Fig. 12. Theoretical velocity curves for the undamaged and the damaged GFRP composite (wave propagation in π_{13} plane).

In particular, in Fig. 12 we show the reconstructions of the theoretical velocity curves for the undamaged and the fatigue post-LVI damaged GFRP sample, respectively, for wave propagation in the plane π_{13}. These curves are the polar plots of the ultrasonic phase velocities calculated starting from the estimated elastic constants collected in Tables 1-2; this theoretical reconstruction of the velocity curves allows for extrapolate the experimental results to angles of propagation wider than those examined during the tests. In Fig. 12, solid lines refer to the undamaged sample, and dotted

lines to the damaged sample; the depicted velocity curves correspond to quasi-longitudinal waves, to quasi-transverse waves and to pure transverse waves.

From the comparison between the velocity curves for the undamaged and the damaged composite, we observe a phase velocities reduction for quasi-longitudinal waves and quasi-transversal waves. On the other hand, the velocity of pure transversal waves remains practically unchanged (except near the x_3-axis). Moreover, we notice that either for the undamaged or for the damaged composite pure transversal waves and quasi-transversal waves have the same velocity along the x_3-axis: hence, we infer that the x_3-axis remains an acoustic axis (material symmetry axis) for the composite even after the damage.

Fig. 13 shows the reconstruction of the theoretical slowness curves for the undamaged and the fatigue post-LVI damaged GFRP sample, respectively, for wave propagation in the plane π_{13}. Also in this case, these curves represent the slowness of ultrasonic waves calculated starting from the estimated elastic constants collected in Tables 1-2. In particular, solid lines refer to the undamaged sample, and dotted lines to the damaged sample; the curves in Fig. 13 correspond to quasi-longitudinal waves, to quasi-transverse waves and to pure transverse waves.

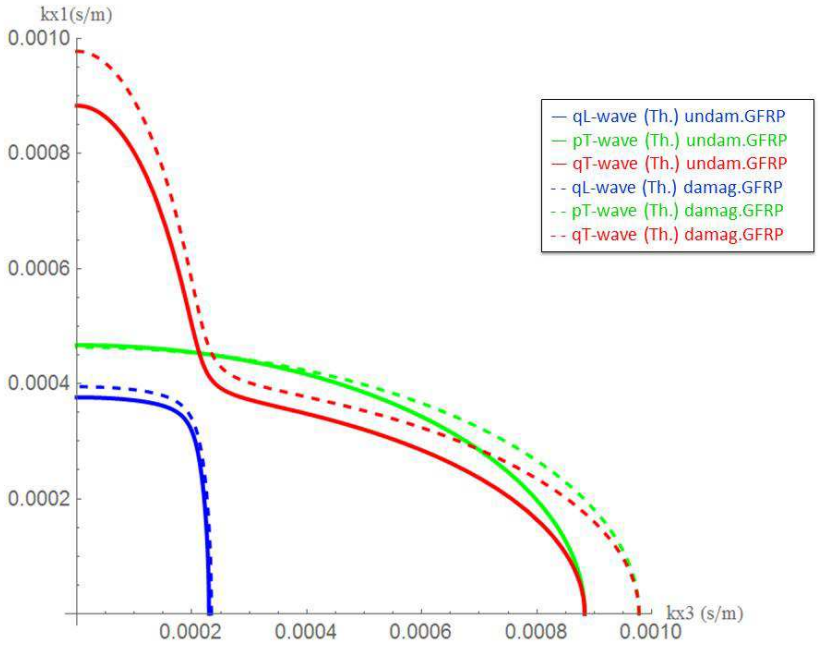

Fig. 13. Theoretical slowness curves for the undamaged and the damaged GFRP composite (wave propagation in π_{13} plane).

Finally, Fig. 14 shows the portion of the slowness curves in the plane π_{13} for the undamaged and the fatigue post-LVI test damaged GFRP sample, obtained by plotting the experimentally determined slowness as a function of the propagation angle, for each possible polarization (quasi-longitudinal,

quasi-transverse and pure transverse waves). Both the theoretical slowness curves (Fig. 13) and the experimental slowness curves (Fig. 14) show an increase of the slowness of quasi-longitudinal waves for the damaged composite, especially near the direction of the x_1-axis (direction of the impact). For what concerns pure transversal waves, within the range of propagation angles experimentally investigated the experimental slowness curves (Fig. 14) show almost the same values of the slowness both for the undamaged and for the damaged sample. Anyway, the theoretical reconstruction of the slowness curves (Fig. 13) shows that the slowness of pure shear waves are similar for the undamaged and the for damaged composite only near the x_1-axis, whereas these slowness differ considerably near the x_3-axis, where we notice a remarkable increase of the slowness due to the damage. Finally, the experimental slowness curves for quasi-transversal waves (Fig. 14) show an increase of the slowness due to the damage in the range of the experimentally investigated propagation angles. The theoretical reconstruction of the slowness curves for quasi-transversal waves (Fig. 13) confirms an increase of the slowness due to the damage for each propagation angle.

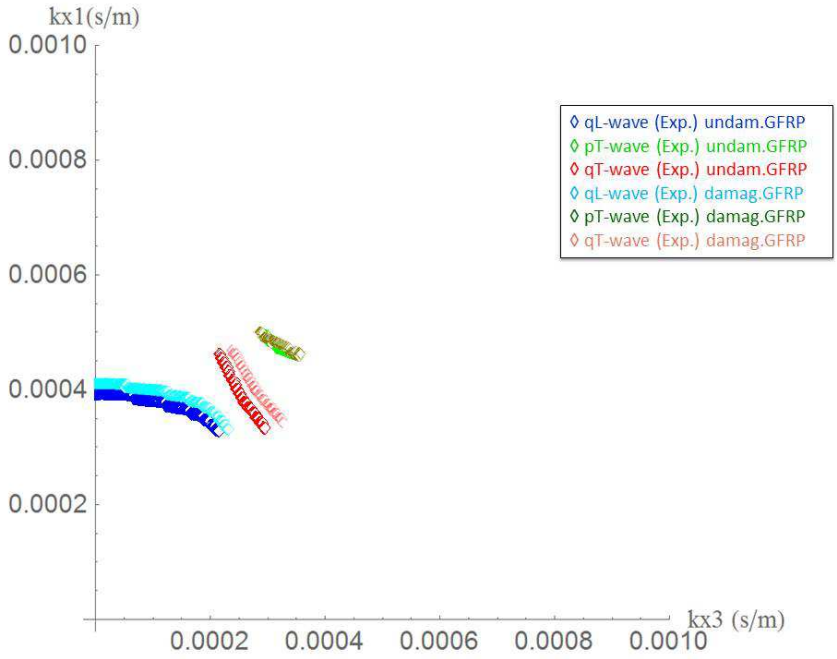

Fig. 14. Experimental slowness curves for the undamaged and the damaged GFRP composite (wave propagation in π_{13} plane).

In conclusion, we may argue that after the fatigue post-LVI damage, all the examined slowness curves show a change in their shapes. In particular, the change induced by the damage on the slowness curve related to quasi-transversal waves indicates an increase of the anisotropy degree in both the directions of the x_1-axis (direction of the impact) and of the x_3-axis (direction of the fatigue

loads). The variation of the slowness curve related to quasi-longitudinal waves indicates an increase of the anisotropy degree only in the direction of the x_1-axis, whereas change of the slowness curve related to pure transversal waves indicates an increase of the anisotropy degree only in the direction of the x_3-axis. It would be interesting to further deepen the analysis of the features of the change of shape of the slowness curves in light of micromechanical analyses of the occurred damage.

Moreover, the fact that the slowness of transversal waves (pure and quasi) propagating along the x_3-axis do not vary after the damage leads to the conclusion that x_3-axis remains an acoustic axis (material symmetry axis) for the composite, even after the damage (as we observed speaking about Fig. 12). This confirms the observation contained in Sect. 3.5, i.e. that the damage appears to have given rise to a fracture only of the Polyester matrix and not of the fibers.

5. Conclusions

In this paper, we propose an experimental approach for ultrasonically characterizing the damage in polymer composites. In particular, the examined damage consist both in a (concentrate) damage due to a low velocity impact, and in a subsequent (diffuse) damage due to fatigue loads. Since the constitutive anisotropy of polymer composites, in our approach the damage is associated to the damage induced anisotropy superimposed to the constitutive anisotropy of the material.

For effectively facing the above problem, we use a suitable ultrasonic goniometric immersion device designed and built at our laboratory, which allows us for determining the velocities of waves travelling in different directions into the composite and having different polarizations. This enables us for analyzing the changes of the anisotropic features of the acoustic response and the variations of the elastic constants due to the damage.

The accuracy in the polar scan of our device allows us for determining the velocity of all possible kind of polarizations: this enhance the precision of the obtainable results with respect to other approaches in the literature, both for the characterization of the constitutive anisotropy and for the characterization of the changes due to the damage.

For what concerns the elastic constants easily accessible by conventional mechanical tests, we have validated the reliability of the results obtained by our ultrasonic procedure by the comparison with the results obtained in tensile tests.

For understanding the features of the damage induced anisotropy it is very helpful the analysis of the changes of the theoretical and experimental characteristic acoustic curves (velocity curves and slowness curves) due to the damage.

A quantitative evaluation of the damage is performed by using an anisotropic damage model developed in the framework of the Continuum Damage Mechanics theory, and based on a tensorial damage measure.

We observe that our approach do not require any a priori assumption on the anisotropy degree of the material and on the orientation of the axes of material symmetry, unlike other experimental methods.

By high accuracy goniometric ultrasonic immersion tests it is also possible to gather information that can be useful for understanding which kind of damage has occurred (matrix cracks, fibers rupture, debonding, etc.). For example, in our experiments the graph phase velocity-incident angle in Fig. 9 shows some unexpected discontinuities in the velocity measurements, and we hypothesized that this is a symptom of discontinuities in the matrix due to the LVI damage. Thus, an interesting subject for future developments is that of correlate the results of goniometric ultrasonic immersion tests with the results of suitable micromechanical investigations. Moreover, our approach has proved to be effective for applications to plane composite specimen of small thickness; we are studying also the possibility of employing the same experimental procedure to thick composites like, for example, those studied for innovative applications in Seismic Engineering [40], and for curved composites like, for example, those employed for structural strengthening [41].

Acknowledgments. We gratefully acknowledge Professor Stéphane Baste for the valuable discussion on the issue of the anisotropic damage of composites. This work was supported by MIUR PON_02 "*MASSIME – Sistemi di sicurezza meccatronici innovativi (cablati e wireless) per applicazioni ferroviarie, aerospaziali e robotiche*" research project.

References

[1] Awaja F, Zhang S, Tripathi M, Nikiforov A, Pugno N. Cracks, microcracks and fracture in polymer structures: Formation, detection, autonomic repair. Progress in Material Science 2016; 83: 536-573.

[2] Bohm K, Gude M, Hufenbach W. A phenomenologically based damage model for textile composites with crimped reinforcement. Composites Science and Technology 2012: 70: 81–88.

[3] Castellano A, Fraddosio A, Marzano S, Piccioni MD. The ultrasonic C-Scan technique for damage evaluation of GFRP composite materials. International Journal of Mechanics 2016; 10: 206-212.

[4] Palumbo D, De Finis R, Demelio GP, Galietti U. A new rapid thermographic method to assess the fatigue limit in GFRP composites. Composites: Part B 2016; 103: 60-67.

[5] Palumbo D, Galietti U. Damage Investigation in Composite Materials by Means of New Thermal Data Processing Procedures. Strain 2016; 52(4): 276-285.

[6] Carvelli V, Feo L, Pegoretti A, Quaresimin M, Zappalorto M. Advances in damage mechanics of polymer composites. Composites: Part B 2014; 65: 1.

[7] Luciano R, Willis JR. Non-local constitutive response of a random laminate subjected to configuration-dependent body force. Journal of the Mechanics and Physics of Solids 2001; 49(2): 431-444.

[8] Barretta R, Luciano R, Willis JR. On torsion of random composite beams. Composite Structures 2015; 132: 915-922.

[9] Barretta R, Luciano R. Analogies between Kirchhoff plates and functionally graded Saint-Venant beams under torsion. Continuum Mechanics and Thermodynamics 2015; 27: 499-505.

[10] Barretta R, Luciano R. Exact solutions of isotropic viscoelastic functionally graded Kirchhoff plates. Composite Structures 2014; 118: 448-454.

[11] Barretta R, Luciano R, Marotti De Sciarra F. A fully gradient model for Euler-Bernoulli nanobeams. Mathematical Problems in Engineering 2015; 2015: 1-8 Article ID 495095, doi: 10.1155/2015/495095.

[12] Panettieri E, Fanteria D, Montemurro M, Froustey C. Low-velocity impact tests on carbon/epoxy composite laminates: A benchmark study. Composites: Part B 2017; 107: 9-21.

[13] Kersemans M, Martens A, Degrieck J, Van D. Abeele K, Delrue S, Pyl L, Zastavnik F, Sol H, Paepegem W. The Ultrasonic Polar Scan for Composite Characterization and Damage Assessment: Past, Present and Future. Applied Science 2016; 6 (2):1-15

[14] Harizi W, Chaki S, Bourse G, Ourak M. Mechanical damage characterization of glass fiber – reinforced polymer laminates by ultrasonic maps. Composites: Part B 2015; 70: 131 - 137

[15] Baste S, Audoin, B. Ultrasonic evaluation of stiffness tensor changes and associated anisotropic damage in a ceramics matrix composite. Journal of Applied Mechanics 1994; 61: 309-16.

[16] Baste S, Aristegui C. Induced anisotropy and crack systems orientations of a ceramic matrix composite under off-principal axis loading. Mechanics of Materials 1998; 29: 19-41.

[17] Margueres Ph, Meraghni F. Comparison of stiffness measurements and damage investigation techniques for a fatigued and post-impact fatigued GFRP composite obtained by RTM process, Composites Part A: Applied Science & Manufacturing 2013; 45: 134-144.

[18] Margueres Ph, Meraghni F. Damage induced anisotropy and stiffness reduction evaluation in composite materials using ultrasonic wave transmission. Composites Part A: Applied Science & Manufacturing 2013; 45: 134-144.

[19] Castellano A, Fraddosio A, Marzano S, Piccioni MD. Un nuovo approccio teorico e sperimentale alla caratterizzazione dell'anisotropia indotta da danno nei materiali compositi fibro-rinforzati. In AIAS – Associazione Italiana Per L'analisi Delle Sollecitazioni 45° Convegno Nazionale Proceedings, Università Degli Studi Di Trieste, Italy, September 7-10, 2016.

[20] Castellano A, Foti P, Fraddosio A, Marzano S, Piccioni MD. A New Ultrasonic Immersion Technique for the Evaluation of Damage Induced Anisotropy in Composite Materials. 3rd International Balkans Conference on Challenges of Civil Engineering, 3-BCCCE, 19-21 May 2016, Epoka University, Albania, Tirana.

[21] Castellano A, Foti P, Fraddosio A, Marzano S, Piccioni MD. Mechanical Characterization of CFRP Composites by Ultrasonic Immersion Tests: Experimental and Numerical Approaches. Composites: Part B 2014; 66: 299–310.

[22] Castellano A, Foti P, Fraddosio A, Marzano S, Piccioni MD. Ultrasonic Immersion Tests for Mechanical Characterization of Multilayered Anisotropic Materials. In: EESMS 2014, 2014 IEEE Workshop in Environmental, Energy and Structural Monitoring Systems Proceedings, Naples, Italy, September 17-18, 2014.

[23] Podymova NB, Karabutov AA, Kobeleva LI, Chernyshova TA. Quantitative Evaluation of the Effect of Porosity on the Local Young's Modulus of Isotropic Composites by Using the Laser Optoacoustic Method. Mechanics of Composite Materials 2013; 49(4): 411-420.

[24] Gurtin ME. The linear theory of elasticity. Encyclopedia of Physics VIa/2. S. Flügge Ed., Springer – Verlag; 1972.

[25] Auld BA. Acoustic fields and waves in solids I. John Wiley & Sons; 1973.

[26] Royer D, Dieulesaint D. Elastic waves in solids I. Free and guided propagation. Springer; 1996.

[27] Payton RG. Elastic Wave Propagation in Transversely Isotropic Media. Kluwer Academic Publishers; 1983.

[28] Castagnède B, Jenkins JT, Sachse W, Baste S. Optimal determination of elastic constants of composite materials from ultrasonic wave speed measurements. J. Appl. Phys. 1990; 67 (6): 2753-2761.

[29] Aristégui C, Baste S. Optimal recovery of the elasticity tensor of general anisotropic materials from ultrasonic velocity data. J. Acoust. Soc. Am. 1997; 101: 813-833.

[30] Castellano A, Foti P, Fraddosio A, Marzano S, Piccioni MD. Mechanical Characterization of Apricena Marble by Ultrasonic Immersion Tests. Key Engineering Materials 2014; 628: 109-116.

[31] Neuenschwander J, Furrer R, Roemmeler A. Application of air-coupled ultrasonics for the characterization of polymer and polymer-matrix composite samples. Polymer Testing 2016; 56: 378-386.

[32] Siva Shashidhara Reddy S, Balasubramaniam K, Krishnamurthy CV, Shankar M. Ultrasonic goniometry immersion techniques for the measurement of elastic moduli. Composite Structures 2005; 67 (1): 3-17.

[33] Hufenbach W, Ritschel T, Bohm R, Langkamp, A. Ultrasonic determination of anisotropic damage in fibre and textile reinforced composite materials. In: Proc. of the Conference on Damage in Composite Materials: Non Destructive Testing and Simulation (CDCM06), 18-19 september, Stuttgart, 2006.

[34] Baste S, Audoin B. On internal variables in anisotropic damage. European Journal of Mechanics A/ Solids 1991; 10 (6): 587-606.

[35] Guerjouma R El, Ducret D, Baboux JC. Ultrasonic study of the anisotropic damage of unidirectional glass-epoxy composites during hygrothermal ageing. In: Proc. of International Committee on Composite Materials (ICCM 12), 1999.

[36] Grippon E, Baste S, Martin E, Aristegui C, Couegnat G. Damage characterization of ceramic matrix composites. In: Proc. of the 15th European Conference on Composite Materials (ECCM 15), 24-28 june, 2012, Venice, Italy.

[37] Krajcinovic D. Continuum Damage Mechanics. Appl. Mech. Rev. 1984; 37 (1): 1-6.

[38] Lemaitre, J. A course on damage mechanics, Springer – Verlag, New York, 1992.

[39] Murakami S. Anisotropic aspects of material damage and application of continuum damage mechanics. In Krajcinovic D, Lemaitre J (Eds) Continuum Damage Mechanics. Theory and Applications. 1987: 91-133.

[40] Castellano A, Foti P, Fraddosio A, Mininno G, Marzano S, Piccioni MD. Seismic Response of a Historic Masonry Construction Isolated by Stable Unbonded Fiber-Reinforced Elastomeric Isolators (SU-FREI). Key Engineering Materials 2014; 628: 160-167.

[41] Caporale A, Feo L, Hui D, Luciano, R. Debonding of FRP in multi-span masonry arch structures via limit analysis. Composite Structures 2014; 108(1): 856-865.

Appendix A

Since ultrasonic signals employed in the experiments are wave packets, for a theoretical overview of the characteristic acoustic surfaces in Sect. 2.2 it is convenient to define the *phase velocity* v, the *group velocity* $\mathbf{v}^g$ and the *energy velocity* $\mathbf{v}^e$ for an acoustic wave propagating in a direction **n** and having polarization **a**.

The *phase velocity* v is the velocity of the wavefront in the direction normal to the wavefront; then, it is possible to define a *phase velocity vector* $\mathbf{v}=v\mathbf{n}$. Of course, the phase velocity coincides with the propagation velocity in case of monochromatic waves, like (1). The *group velocity* $\mathbf{v}^g$ is the propagation velocity of the wave packet, and indicates the energy flow direction. The group velocity is also named *ray velocity*, and it is defined as:

$$\mathbf{v}^g = \frac{\partial \omega}{\partial \mathbf{k}}, \qquad \mathbf{k} = k\mathbf{n} \tag{A.1}$$

with ω the angular frequency of the wave packet, and **k** the wave vector.

When ultrasonic waves propagate in isotropic materials, the phase velocity vector **v** coincides with the group velocity $\mathbf{v}^g$. Instead, when ultrasonic waves propagate in anisotropic materials, a beam divergence occurs, and the phase velocity vector **v** is generally different from the group velocity $\mathbf{v}^g$, unless the propagation direction does not coincide with a material symmetry axis. The deviation between the directions of the phase velocity vector **v** and of the group velocity vector $\mathbf{v}^g$, named *beam skewing*, is measured through the *skewing angle* ψ (Fig. A.1).

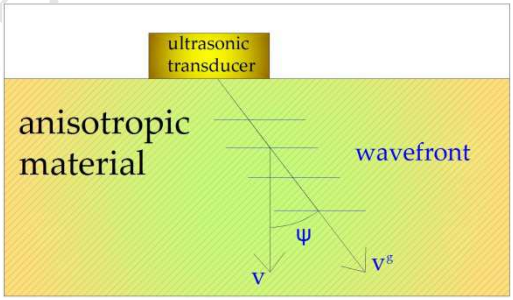

Fig. A.1. Plane waves propagating in anisotropic materials: deviation between the group velocity and the phase velocity vector.

The *energy velocity* $\mathbf{v}^e$ is given by the Poynting vector related to the propagation of the wave divided by the total energy per unit volume. It is possible to show that $\mathbf{v}^e$ has the following expression:

$$\mathbf{v}^e = \frac{\mathbb{C}\left[\mathbf{a} \otimes \mathbf{n}\right]\mathbf{a}}{\rho \, \mathrm{v} \, \mathbf{a} \cdot \mathbf{a}} \tag{A.2}$$

For a displacement with unit magnitude ($|\mathbf{a}| = 1$), the energy velocity becomes

$$\mathbf{v}^{e,1} = \frac{\mathbb{C}\left[\mathbf{a} \otimes \mathbf{n}\right]\mathbf{a}}{\rho \, \mathrm{v}} \tag{A.3}$$

The energy velocity $\mathbf{v}^e$ point the direction of the "acoustic ray", that is the direction of energy transport [21]. When the acoustic ray is perpendicular to the wavefront, and therefore parallel to **n**, the mode of wave propagation is a "pure" mode (notice that this definition encompass a broader class of waves than pure longitudinal or pure transverse waves).

By the scalar product between $\mathbf{v}^{e,1}$ and **n**, we obtain, also recalling the minor symmetries properties of $\mathbb{C}$:

$$\mathbf{v}^{e,1} \cdot \mathbf{n} = \frac{\mathbb{C}\left[\mathbf{a} \otimes \mathbf{n}\right]\mathbf{n} \cdot \mathbf{a}}{\rho \, \mathrm{v}} \tag{A.4}$$

from which by (3) we get:

$$\mathbf{v}^{e,1} \cdot \mathbf{n} = \mathrm{v} \tag{A.5}$$

Then, for a plane wave, the projection of the energy velocity $\mathbf{v}^{e,1}$ in the propagation direction **n** is equal to the phase velocity.

Moreover, it is possible to compare the energy velocity with the group velocity. Indeed, in view of (4) the condition for the existence of non-trivial solution of the Christoffel equation (3) is:

$$\det\left[\mathbb{C}^{\mathrm{t}}\left[\mathbf{n} \otimes \mathbf{n}\right] - \rho \mathrm{v}^2 \mathbf{I}\right] = 0, \tag{A.6}$$

which relates the phase velocity v to the direction of propagation **n**. Multiplying (A.6) by k^6 (see [21]), we obtain

$$\det\left[\mathbf{\Gamma}^{t}\left[k\mathbf{n}\otimes k\mathbf{n}\right]-\rho v^2k^2\mathbf{I}\right]=0 \tag{A.7}$$

where: k**n**=**k** and kv=ω. Then, the dependence of the angular frequency ω on **k** is the same as the dependence of the phase velocity v on **n**; this imply by (A.1) that

$$\mathbf{v}^{g}=\frac{\partial\omega}{\partial\mathbf{k}}=\frac{\partial v}{\partial\mathbf{n}}. \tag{A.8}$$

It is possible to determine $\frac{\partial v}{\partial\mathbf{n}}$ by differentiating v^2, and by using the Fresnel-Hadamard condition (3); indeed, after few passages, we get:

$$2v\,\frac{\partial v}{\partial\mathbf{n}}=\frac{\mathbf{\Gamma}\left[\mathbf{a}\otimes\mathbf{n}\right]\mathbf{a}}{\rho\,\mathbf{a}\cdot\mathbf{a}} \tag{A.9}$$

whence, by (A.2) and (A.8) we have:

$$\mathbf{v}^{g}=\frac{\mathbf{\Gamma}\left[\mathbf{a}\otimes\mathbf{n}\right]\mathbf{a}}{\rho\,v\,\mathbf{a}\cdot\mathbf{a}}=\mathbf{v}^{e}. \tag{A.10}$$

Then, the group velocity $\mathbf{v}^g$ is equal to the energy velocity $\mathbf{v}^e$.